CLOUD-MODEL BASED BAYESIAN TECHNIQUES FOR PRECIPITATION PROFILE RETRIEVAL FROM TRMM MICROWAVE SENSORS

A. Mugnai [1], S. Di Michele [1,2], F.S. Marzano [3], A. Tassa [1,2]

[1] *Istituto di Fisica dell'Atmosfera, Consiglio Nazionale delle Ricerche*
Via Fosso del Cavaliere 100 – 00133 Roma, Italy
E-mail: Alberto.Mugnai@ifa.rm.cnr.it

[2] *Fondazione per la Meteorologia Applicata*
Via Caproni 8 – 50145 Firenze, Italy
E-mail: Sabatino.DiMichele@ifa.rm.cnr.it, Alessandra.Tassa@ifa.rm.cnr.it

[3] *Dipartimento di Ingegneria Elettrica, Università dell'Aquila*
Monteluco di Roio – 67040 L'Aquila, Italy
E-mail: marzano@ing.univaq.it

Abstract. A statistical retrieval technique for estimating precipitation cloud profiles from TRMM measurements has been developed. The inversion method is based on the Bayesian estimation theory and implemented by means of the Minimum Mean Square criterion. The retrieval technique, named Bayesian Algorithm for Microwave-based Precipitation Retrieval (BAMPR) is trained by a three-dimensional (3-D) cloud-radiation database, generated by inputting the numerical outputs of a mesoscale cloud-resolving model into a 3-D radiative transfer model. Retrieval products are the hydrometeor and precipitation rate profiles together with columnar equivalent water contents and surface rainrates. Microphysical and radiative aspects of the forward problem are investigated, pointing out critical aspects and further refinements of the proposed technique. Two separate algorithms using the same framework have been developed: an algorithm for TMI data only (BAMPR-P, where "P" stands for passive), and a combined algorithm that uses both TMI and PR data (BAMPR-C). Applications of the two retrieval methods to TRMM data concentrate on the case of the Hurricane Bonnie on August 25, 1998, which is analyzed and discussed in detail by using TRMM official products as a comparison.

1 Introduction

Retrieval of precipitation profiles from spaceborne microwave sensors has received a new incentive after the launch of the Tropical Rainfall Measuring Mission (TRMM) platform in 1997 (Kummerow et al., 1998). The coexistence of the TRMM Microwave Imager (TMI) and Precipitation Radar (PR) instruments aboard TRMM represents an unprecedented opportunity to exploit, and possibly to merge, passive and active spaceborne microwave measurements.

Several inversion techniques have been proposed and applied in the last two decades for estimating cloud and precipitation parameters from measurements taken by space-borne microwave radiometers -- especially, the Special Sensor Microwave/Imagers (SSM/Is) flown aboard spacecraft of the U.S. Defense Meteorological Satellite Program (DMSP) (see Wilheit et al., 1994 and Smith et al., 1998 for comprehensive descriptions of several SSM/I algorithms). Among these techniques, we enumerate the approaches based on multiple regression and on Maximum Likelihood methods. Recently, Bayesian techniques have been proved to have a large potential and flexibility for precipitation profiling (Evans et al., 1995; Pierdicca et al., 1996; Marzano et al., 1999). Their unique feature is that they constitute a rigorous statistical framework in which to develop cloud-model based inversion methods and combined multisensor approaches. As opposed to empirical methods where measurements of both brightness temperatures and precipitation parameters are collected to train a retrieval algorithm, the model-based approaches resort to refined physical models to simulate the measurements (Mugnai et al., 1990; Smith et al., 1992; Mugnai et al., 1993; Smith et al., 1994a, 1994b; Kummerow et al., 1996). This point of view offers the possibility to avoid *in situ* measurements and to deepen

the understanding of the problem. On the other hand, model-based approaches have to tackle the critical issue of tuning simulations to the measurement manifolds in order to be representative of real observations (Marzano et al., 1994; Panegrossi et al., 1998).

Following the Tropical Ocean Global Atmosphere – Coupled Ocean Atmosphere Response Experiment (TOGA-COARE) in 1993, several researches have dealt with the comparison of contemporary active and passive microwave observations of precipitation; however, relatively few attempts have been made in order to combine radar and radiometer measurements within the same precipitation retrieval scheme (Meneghini et al., 1994; Schols and Weinman, 1994, Marzano et al., 1995; Olson et al., 1996; Haddad et al., 1997; Marzano et al., 1999). On one hand, radiometer measurements can be used to properly account for the contamination of radar echoes due to fairly strong hydrometeor attenuation at frequencies above 10 GHz (Iguchi and Meneghini, 1994; Meneghini et al., 1997; Smith et al., 1997). On the other hand, the radar range resolution can help the retrieval algorithms to better define the near-surface precipitation vertical profile (Testud et al., 1992; Marzano et al., 1994). The TRMM platform offers a unique opportunity to develop and test algorithms for TMI and PR combined precipitation retrieval, even though the different scanning geometry of the two instruments has to be carefully taken into account.

In this work, we describe the methodological features of Bayesian algorithms trained by three-dimensional (3-D) dynamical cloud-resolving model outputs combined with 3-D radiative transfer models. Microphysical and radiative aspects of the forward problem will be also discussed. Finally, applications of the precipitation retrieval methods to TRMM data will be shown. In particular, the case of the Hurricane Bonnie on August 25, 1998 will be analyzed and discussed in detail.

2 Retrieval schemes

The block-diagram of the Bayesian Rainfall Algorithm for Microwave Sensors (BAMPR) is shown in Figs. 1 and 2 for single-sensor (radiometer, BAMPR-P) and for combined sensors (radiometer plus radar, BAMPR-C) cases, respectively.

2.1 Using single sensor (TMI)

In Fig. 1, the two grey-contoured boxes refer to the two main blocks common to all physically-based retrieval approaches (Mugnai et al., 1993; Smith et al., 1994a; Pierdicca et al., 1996; Kummerow et al., 1996). They are generally referred to as the "forward problem" and the "inverse problem".

The *forward problem* consists in the generation of a database, in which the simulated brightness temperatures (TBs) that would be measured by a space-borne radiometer, are associated to the various cloud structures generated by a cloud-resolving model. The *cloud-radiation database generation* block accounts for the simulation of the upwelling TBs corresponding to each cloud structure. In the proposed scheme, we associate to each set of TBs a slanted profile (according to the 53.1° viewing angle of the radiometer) at the resolution of the 37 GHz channels. This association is not straightforward, especially in the case of a 3-D geometry approach as explained in Sub-section 3.2.1. The spatial correlation matrix is also computed by considering the spatial variability of the simulated TBs at the various channel resolutions within the simulated scenario. The output of the forward-modeling procedure is the construction of a statistically significant cloud-radiation database.

In the *inverse problem*, the cloud-radiation database is therefore used to train the Bayesian inversion algorithm, whose products are the hydrometeor and precipitation rate profiles together with the hydrometeor columnar contents and the surface rainrates (Marzano et al., 1999). The Bayesian technique has been applied by resorting to the Minimum Mean Square (MMS) criterion, which will be described in Section 4.

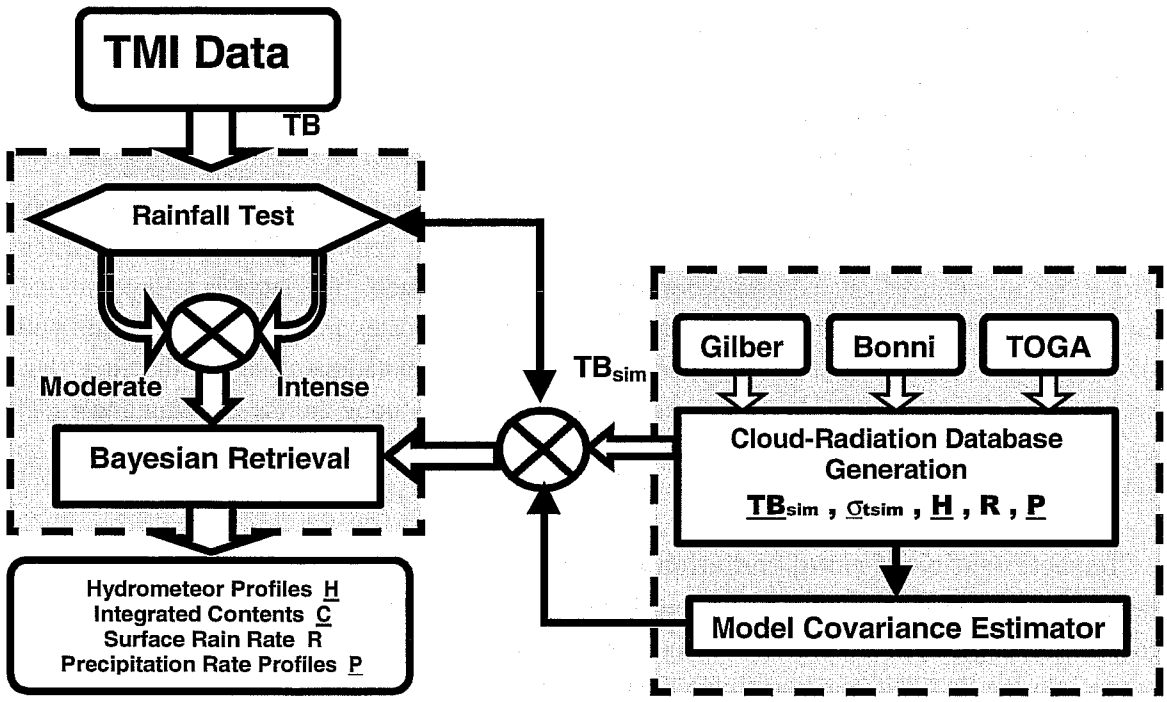

Fig 1: Scheme of the Bayesian Algorithm for Microwave-based Precipitation Retrieval for TMI precipitation profile retrieval (BAMPR-P). TB_{sim} stands for the simulated TBs, while σ_{tsim} stands for their spatial variations.

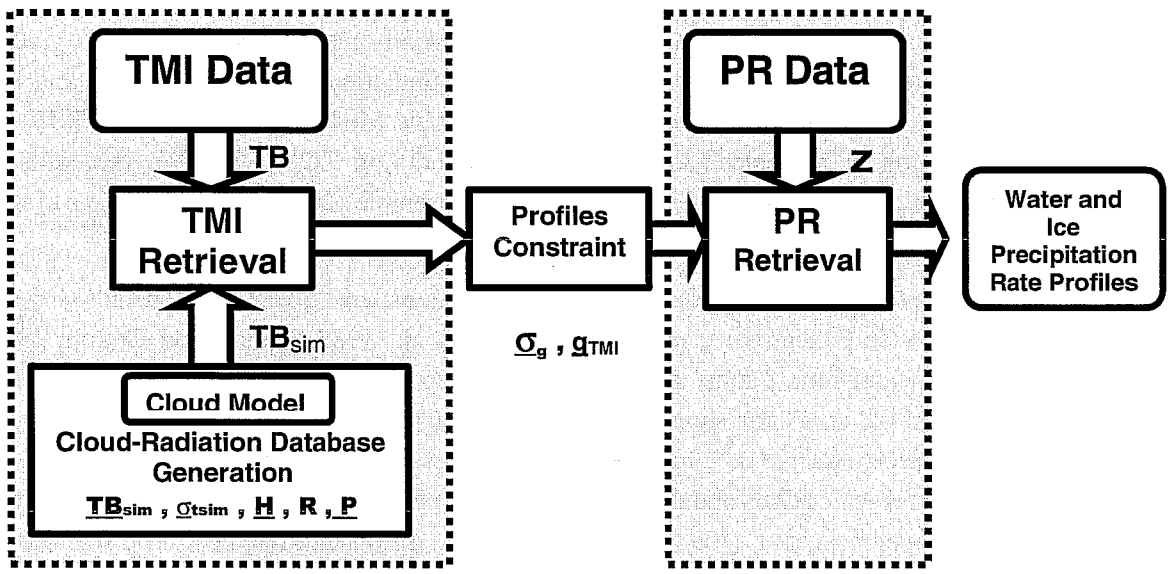

Fig 2: Scheme of the Bayesian Algorithm for Microwave-based Precipitation Retrieval for TMI-PR combined precipitation profile retrieval (BAMPR-C). g_{TMI} stands for the TMI-only estimated hydrometeor profiles and σ_g stands for their uncertainties.

2.2 Using combined sensors (TMI and PR)

In our approach, the development of a new combined precipitation retrieval method to be applied to TRMM radar and radiometric measurements is achieved by means of a two-step Bayesian approach. As already noted, TRMM scanning geometry makes any direct use of combined TMI and PR measurements very complex.

As shown in Fig. 2, the algorithm first step is based on TMI data and trained by a cloud-radiation database, quite analogously to the TMI algorithm shown in Fig. 1. However, here the TMI-retrieved profiles and their standard deviations are used as a constraint for the second cascade step. The latter is a Bayesian technique as well, in which the PR measurements and the TMI-based profile estimates are used in conjunction with a cloud-reflectivity database, that is built from the same cloud model simulations used for the first step. In this process, the TMI-estimated slanted profiles need to be re-projected along the PR pointing angle. The typical output is given by the estimates of the precipitation rate profiles at PR ground-resolution and of the corresponding hydrometeor equivalent water contents.

3. Characterization of cloud-radiation databases

For the TMI precipitation profile retrieval, the cloud-radiation database consists of a large set (thousands) of slanted precipitating cloud profiles and of the corresponding brightness temperatures at TMI channels and resolutions. In the TMI-PR combined precipitation profile retrieval case, on the other hand, an additional database has to be considered, which consists of vertical precipitating cloud profiles and of the corresponding PR-reflectivity profiles.

3.1 Cloud-radiation database generation

The precipitating cloud structures are based on the outputs of 3-D numerical mesoscale non-hydrostatic cloud-resolving models, which explicitly produce the equivalent water contents of six species of hydrometeors (cloud droplets, raindrops, graupel particles, pristine ice crystals, ice aggregates and snow flakes) as a function of space and time. No explicit indication on the presence of partially melted hydrometeors is given by the models we utilize. At present, we make use of two hurricane simulations (hurricane Gilbert and hurricane Bonnie) generated by the University of Wisconsin - Non-hydrostatic Modeling System (UW-NMS) (Tripoli, 1992), and of a simulation of a tropical squall line observed during TOGA-COARE (hereafter, TOGA simulation), that has been produced by the Goddard Cumulus Ensemble (GCE) cloud modeling system (Tao and Soong, 1986).

In the UW-NMS simulations, the hydrometeor size distributions are given by constant-slope inverse exponential distributions (see Panegrossi et al., 1998; Cotton et al., 1982; Tripoli and Cotton, 1980) with slopes equal to 1.852 mm^{-1} for rain, 2 mm^{-1} and 1 mm^{-1} for graupel (for hurricane Bonnie and for hurricane Gilbert, respectively), and 0.3 mm^{-1} for snow and aggregates. Cloud droplets and pristine ice crystals are monodispersed with diameters equal to 0.02 mm and 0.230 mm, respectively. Hydrometeor density is equal to 0.22 g/cm^3 and 0.6 g/cm^3 for ice crystals and graupel particles, respectively, while for snow and ice aggregates it varies with size as in Panegrossi et al. (1998). For the GCE model, constant-intercept drop size distributions are assumed (see Kummerow et al., 1996), with intercepts equal to 8000 $m^{-3}mm^{-1}$ for rain, and 4000 $m^{-3}mm^{-1}$ for graupel, snow and aggregates. Graupel density is 0.4 g/cm^3, while snow density is 0.1g/cm^3. Cloud droplets and cloud ice are monodispersed with diameters equal to 0.1 mm and 0.02 mm, respectively, and ice density is 0.9g/cm^3.

From the outputs of the cloud models, the upwelling brightness temperatures are computed, and the corresponding hydrometeor equivalent liquid water content (LWC) profiles are extracted for the cloud-radiation database. The definition of these cloud profiles, however, is by no means unique, as it will be explained in Sub-section 3.2.1.

The simulated TBs are generated by means of a 3D-adjusted plane-parallel radiative transfer (RT) code (Roberti et al., 1994; Liu et al., 1996; Bauer et al., 1998) at the TMI frequencies and viewing angle (53.1°). The TBs are computed at model resolution (which is generally much higher than the satellite footprints), and then filtered in order to reach the TMI effective resolutions for the different channels. At each frequency, the antenna pattern of the radiometer is simulated by means of a 2-dimensional Gaussian weighting function, where the half-power beam width equals the footprint at that frequency.

In addition to the hydrometeor LWC profiles, the database contains the corresponding precipitation rate profiles for both rain and ice (i.e., graupel and snow). At each altitude, the rain/ice precipitation rate is computed by using the terminal fall velocities given by Flatau et al. (1989) together with the vertical wind speed, temperature and pressure produced by the cloud model, and the rain/ice size distributions used within the RT computations – which may be different from those of the cloud model, as explained in Sub-section 3.2.2. It is worth mentioning that the conversion into precipitation rates makes the comparison of TMI retrievals with radar products almost straightforward.

As an example, Fig. 3 shows, in terms of mean and variance, both the vertical distributions of rain, graupel and snow, and the total (ice + rain) precipitation rate profile for hurricane Bonnie simulation (minute 2130).

For the purpose of comparing the cloud-model reflectivities with the PR-measured ones, we have found it convenient to compute the attenuated average reflectivities due to the various layers of the cloud model (see Sub-section 4.2). The attenuated average reflectivity Z_i (in $mm^6\ m^{-3}$) due to the *i*-th cloud model layer and observed at the platform altitude is given by (Marzano et al., 1999):

$$Z_i\,(z=0) = (Z_{ei} / 2\tau_i)\,[1 - \exp(-2\tau_i)]\,\exp(-2\tau_{io}) \qquad (1)$$

being τ_i the optical thickness of the *i*-th layer, τ_{i0} the optical thickness from the top of the *i*-th layer to the radar antenna altitude (z=0), and Z_{ei} the equivalent reflectivity per unit volume (constant within the *i*-th layer), which is given by :

$$Z_{ei} = \lambda^4\,\pi^{-5}\,|K|^{-2} \int_0^\infty \sigma_b(r)\,N(r)\,dr \qquad (2)$$

where λ is the wavelength, K the refractive-index polarizability ($|K|$ is equal to 0.93 for liquid water at 13.8 GHz), σ_b the back-scattering cross-section and N(r) the particle distribution, with r the particle radius. Moreover, for each cloud layer, the total path attenuation (a, in dB) has been considered as an additional predictor:

$$a = \Sigma_i\ \tau_i \quad \text{with} \quad i=1,N \qquad (3)$$

where N are the radar range bins. As an example, Fig. 4 shows the simulated reflectivies for two vertical sections across the hurricane Bonnie simulation, minute 2130.

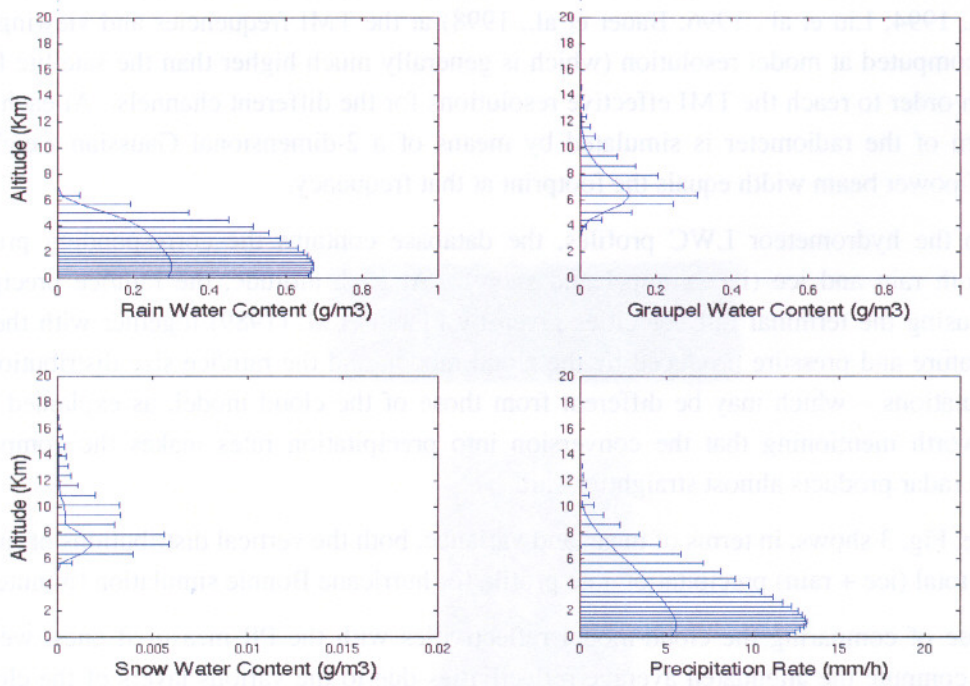

Fig 3: Vertical distributions of rain (upper left panel), graupel (upper right), and snow (lower left) water contents, and of the total precipitation rates (lower right panel) for hurricane Bonnie simulation (minute 2130). At each level, both mean and variance are shown.

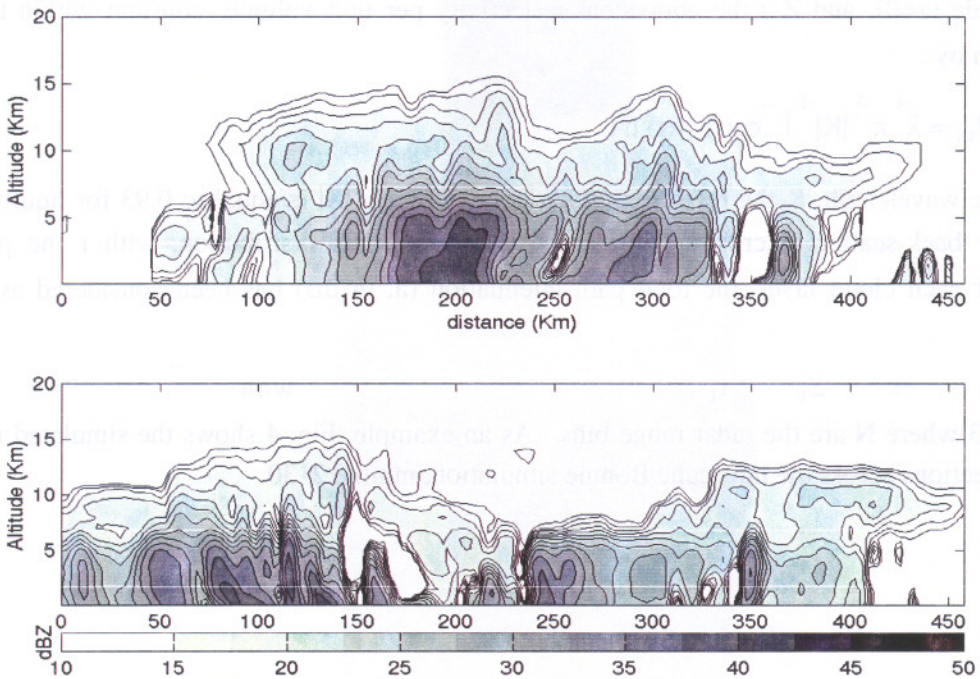

Fig 4: Selected vertical cuts of the simulated reflectivities for hurricane Bonnie simulation (minute 2130). Contour lines are from 10 to 55 dBZ in steps of 2.5 dBZ

As shown in Fig. 1, the database of the simulated TBs is clustered into two separate classes corresponding to moderate and intense precipitation regimes. This classification -- which mitigates the ill-conditioning of the problem and is also useful for speeding up the retrieval -- is unsupervised, i.e. it is based only on the emerging TBs and their variations, rather than on the model microphysics. We recognize that a stratiform/convective classification criterion (see, for instance, Anagnostou and Kummerow, 1997; Mohr et al., 1998; Hong et al., 1999) would probably be a better solution. However, we have found that such criterion is hardly applicable over slanted profiles of the adopted cloud model simulations, because mixed convective and stratiform portions often coexist within the same cloud structure.

It is worth mentioning that before performing the retrieval, it is necessary to check the representativeness of the database for the typology of precipitation event which is under consideration -- i.e., its capability of reproducing that event from a radiative point of view. On a rigorous basis, the retrieval may be performed only if the manifold of the measured TBs and/or reflectivities is completely overlapped by that of the simulations. On the contrary, when the two manifolds are largely different, the precipitation event is not adequately represented by the database (see Panegrossi et al., 1998) and therefore no retrieval should be attempted.

Fig. 5 shows, in terms of frequency-dependent scatterplots, a comparison between the measured TBs for hurricane Bonnie on August 25, 1998, and the simulated ones for the full database (i.e., generated by means of all adopted cloud model simulations). Noteworthy, the simulated TBs show a satisfying agreement with the measurements, especially at the lower frequencies. However, for a few pixels the measured TBs are not matched by the simulations. This is apparent in Fig. 6, where the TMI pixels for hurricane Bonnie that are adequately matched by the 8-dimensional TB-database (i.e., the TB-distance is below a given threshold, which we take as 4 K) are shown as white points, whereas the pixels for which such agreement is not found are represented by the red points, and the black areas correspond to not-rainy or over-land pixels. By defining a Matching Index (MI) as the percentage of white to white+red pixels, we obtain MI = 99% for Figs. 5 and 6.

It is also interesting to consider which portions of the database are used by the algorithm for the retrieval of different events. For instance, in order to evaluate the representativeness of the various cloud model simulations, we associate a Simulation Index (SI) to each retrieved pixel, indicating the relative weight of the simulations within the retrieval process. For simplicity, we define SI as the

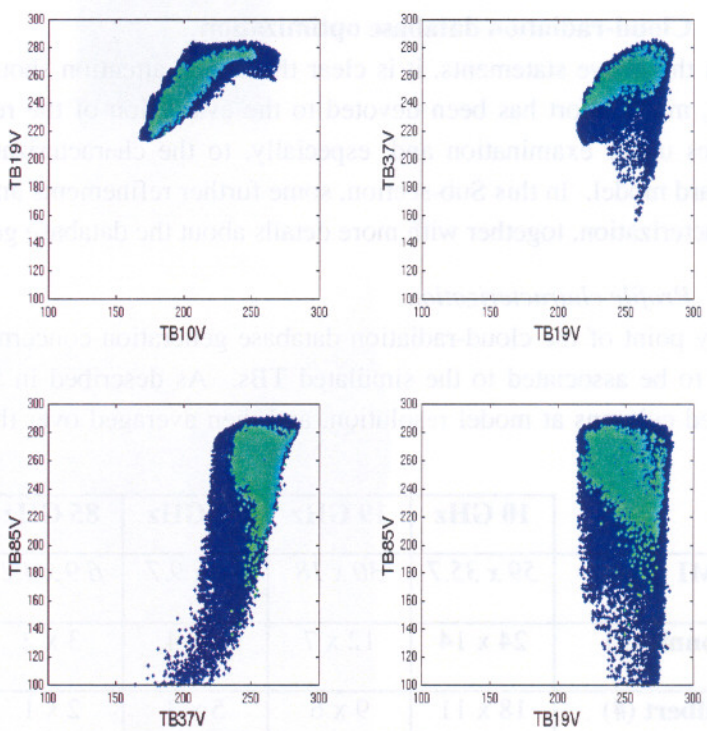

Fig 5: Frequency-dependent scatterplots of the simulated TBs of the full cloud-radiation database (blue points), and of TMI data for hurricane Bonnie, granule 4267 (cian points).

simulation that generates the closest set of TBs with respect to the TMI measurements. We notice, however, that in the MMS approach – that is used in the present report (see Sub-section 4.1) -- it would be more appropriate to consider all points of the database that are used by the retrieval algorithm with their corresponding weights.

Fig. 7 shows the results of this analysis for the Hurricane Bonnie case by using different colors for the different values of Simulation Index, i.e. for the different simulations that have been selected by the algorithm for each pixel. It turns out that for the intense core of the cyclone, the algorithm selects cloud structures provided by the hurricane Bonnie simulation, whereas on the cloud edges the TOGA simulation is preferred. In summary, for this case 89% of the retrieved profiles are taken from the hurricane Bonnie simulation as shown in Table I, which gives the percentages for other case studies as well. Interpretation of these results is not straightforward because the simulated upwelling TBs depend not only on the hydrometeor profiles (which are different for the three simulations), but also on the different beam filling characterization of the simulations, and on the fact that different values of the wind speed have been used to compute the sea surface emissivity.

Database Measurements	BONNIE	GILBERT	TOGA
Bonnie (Granule 4267)	89	1	10
Astrid (Granule 11938)	54	1	45
Atoll (Granule 4176)	0	0	100

Table I: Percentages of the cloud simulation (columns) used for the retrieval of three different case studies (rows), with respect to the total number of rainy pixels.

3.2 Cloud-radiation database optimization

From the above statements, it is clear that much attention should be paid on the generation of the database. Thus, much effort has been devoted to the evaluation of the representativeness of the database for the case studies under examination and, especially, to the characterization of the errors and/or uncertainties of the forward model. In this Sub-section, some further refinements and recommendations are given for the database characterization, together with more details about the database generation.

3.2.1 Profile characterization

A key point of the cloud-radiation database generation concerns the definition of the cloud structures which have to be associated to the simulated TBs. As described in Sub-section 3.1, the TBs are computed along slanted columns at model resolution, and then averaged over the simulated scenario according to the size of the footprints at the various TMI frequencies. Considering that the three cloud model simulations have different horizontal resolutions (2.5 km, 3.3 km, and 1.0 km for hurricane Bonnie, hurricane Gilbert, and TOGA, respectively), a different number of pixels has been considered for computing the averages (see Table II). Noteworthy, this convolution, which is necessary to reproduce the

	10 GHz	19 GHz	37 GHz	85 GHz
TMI (km)	*59 x 35.7*	*30 x 18*	*16 x 9.7*	*6.9 x 4.2*
Bonnie (#)	24 x 14	12 x 7	6 x 4	3 x 2
Gilbert (#)	18 x 11	9 x 6	5 x 3	2 x 1
TOGA (#)	59 x 36	30 x 18	16 x 10	7 x 4

Table II : Number of model pixels required to match the TMI ground resolutions for the three simulations used to generate the cloud-radiation database.

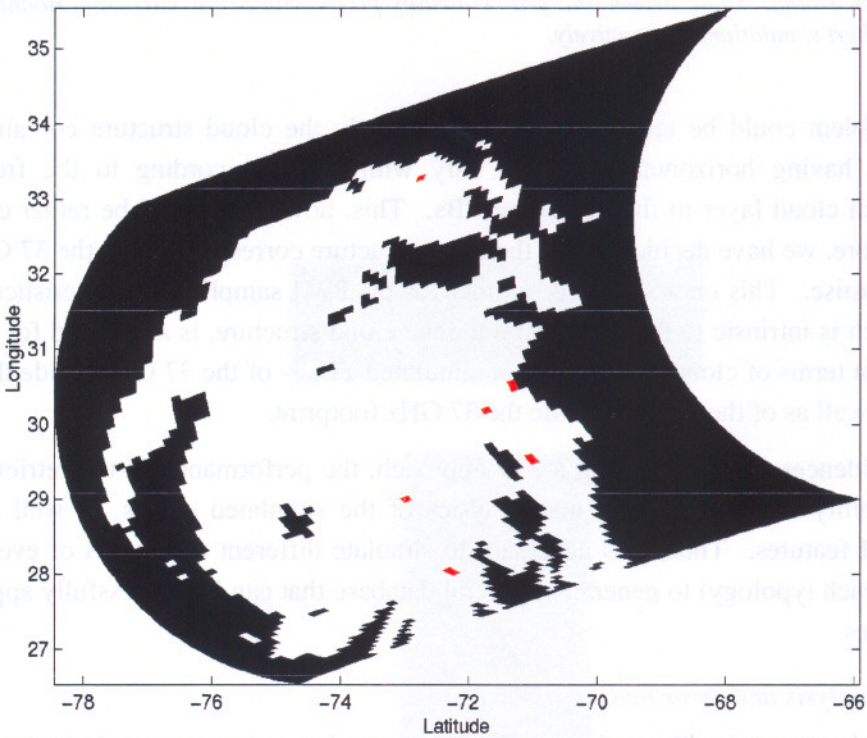

TMI resolutions, makes it difficult to uniquely identify the cloud structure to be associated to each set of simulated TBs, because four different cloud structures -- filling up elliptical cylinders with sizes corresponding to the cross-track and along-track resolutions of the 10, 19, 37 and 85 GHz frequencies -- are actually associated to each point of the database.

Fig 6: Hurricane Bonnie on August 25, 1998 (granule 4267). The black points are not-rainy or over land. The red points are not overlapped by the cloud-radiation database. The white points are overlapped (within 4 K difference). The Matching Index MI is 99%.

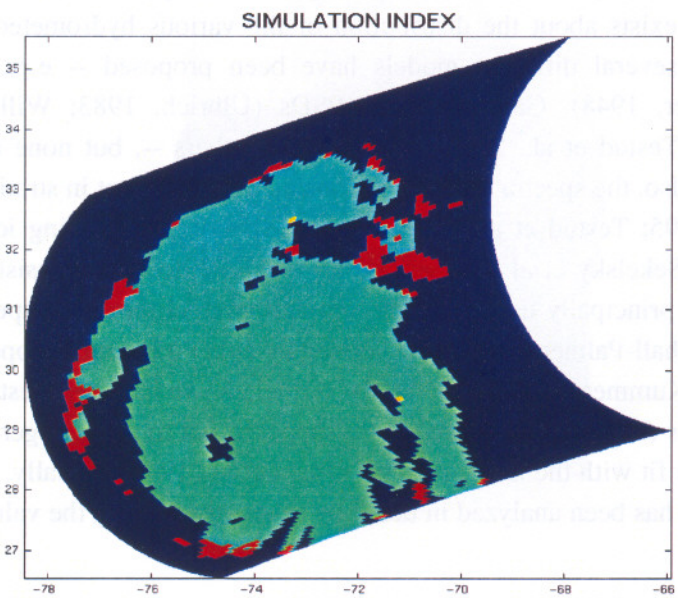

Fig 7: Simulation Index (SI) for hurricane Bonnie on August 25, 1998 (granule 4267). The blue pixels are not-rainy or over-land. Cian, brown and yellow identify pixels with SI for hurricane Bonnie, TOGA and hurricane Gilbert simulations, respectively.

In theory, this problem could be tackled by considering only the cloud structure contained in a deformed elliptical cylinder, having horizontal sizes that vary with height according to the frequency-dependent contribution of each cloud layer to the upwelling TBs. This, however, would be rather complex and pixel-dependent. Therefore, we have decided to use the cloud structure corresponding to the 37 GHz frequency as a reasonable compromise. This choice is also optimal for the TMI sampling characteristics. In addition, the retrieval error which is intrinsic to the choice of a unique cloud structure, is accounted for by considering the variability -- both in terms of cloud profiles and of simulated TBs -- of the 37 GHz inside the footprints of the 19 and 10 GHz, as well as of the 85 GHz inside the 37 GHz footprint.

This discussion evidences that when using a 3-D approach, the performance of the retrieval depends on the cloud model capability to reproduce the microphysics of the simulated events, as well as their horizontal patterns and spatial features. Thus, it is necessary to simulate different typologies of events (and, possibly, several events for each typology) to generate a general database that can be successfully applied to the various precipitation regimes.

3.2.2 Sensitivity analysis and error budget

Several parameters having a significant degree of uncertainty play an important role in the forward modeling. In the RT calculations, for instance, assumptions must be made on important parameters that are not sufficiantly specified within the cloud model. Thus, we have carried out sensitivity tests to evaluate the impact on the upwelling TBs which is due to parameters that determine the surface emissivity or the single scattering properties of the hydrometeors. As a result, model covariance matrices have been built in order to take into account these uncertainties.

The effects, resulting both from our sensitivity tests and from a careful review of the literature, can be summarized as follows (see also Tassa et al., 2001):

- **Particle Size Distributions** (PSDs). As pointed out by Panegrossi et al. (1998), the PSDs are one of the main sources of uncertainty in the simulated brightness temperatures at microwave frequencies. A flourishing literature exists about the distribution of the various hydrometeors with size. For the rain drops, for instance, several different models have been proposed -- e.g., inverse-exponential PSDs (Marshall and Palmer, 1948), Gamma-shaped PSDs (Ulbrich, 1983; Willis and Tattelmann, 1989), "normalized" PSDs (Testud et al., 2000), among many others --, but none of them has yet received a general consensus. Also, the spectra seem to be considerably different in stratiform and convective clouds (Tokai and Short, 1995; Testud et al., 2000). The PSDs of precipitating ice are even more uncertain (Houze et al., 1979; Sekelsky et al., 1999). In our database, to keep consistency with the cloud model simulations, we have principally used for both rain and graupel the PSDs specified by the cloud models themselves: i.e., Marshall-Palmer PSDs characterized by either a constant-slope (Cotton et al., 1982) or by a constant-intercept (Kummerow et al., 1996). Nevertheless, we have also tested truncated constant–slope Marshall-Palmer PSDs (in which the particles are supposed not to grow larger than a maximum diameter) for they allow a better fit with the measurements (Tassa et al., 1999). Finally, the effect of PSD modeling on the upwelling TBs has been analyzed in detail by randomly varying the value of the slope for constant-slope PSDs.
- **Particle Shapes.** In our RT calculations, we have assumed spherical hydrometeors and have therefore used Mie theory to compute their scattering properties. Non-sphericity generates polarization differences

characteristics of the particles themselves (Roberti and Kummerow, 1999). We plan to insert values from the literature into the radiometric-error covariance matrix.

- **Melting Phase.** The effects of melting have not been yet considered because the cloud models do not provide any direct indication on melting ice particles (i.e., on their vertical distribution and melting fraction). In addition, in the case of stratiform precipitation, an accurate parameterization of the melting layer would require a vertical resolution higher than that presently ensured by the dynamical models. This problem has been tackled by Bauer (2000) (see also Bauer et al., 2000), who has found TB increases as large as 8 K at the lower frequencies (10 and 19 GHz) over ocean. These values could be inserted in the radiometric-error covariance matrix as well. Sensitivity studies are planned for using the University of Essex scattering model by melting particles (Walden et al., 1999) into our RT calculations. The insertion of melting particles is obviously expected to play a major role in the calculation of simulated radar reflectivities.

- **Sea Surface Wind Speed.** For the sea-surface emissivity, we have adopted the model developed by the Université Catholique de Louvain (UCL) (Lemaire, 1998), which is function of surface wind velocity and rainrate. Even though clouds and precipitation tend to hide the impact of surface characteristics on the upwelling TBs, this effect can be significant at the lower frequencies in the case of low rainfall rates (we compute TB differences at 10 GHz that may be as large as about 20 K and 10 K for horizontal and vertical polarization, respectively, when surface emissivity characteristics are changed). Moreover, at these frequencies, pixels at the cloud edges usually contain both cloudy and cloud-free areas, thus enhancing the impact of surface emissivity. We have carried out sensitivity tests to explore these effects. It turns out that while the rainfall-induced ring waves have a negligible impact on the upwelling TBs, the effects due to wind speed may be quite important accounting for most of the computed TB variations. In our studies, this latter effect is taken into account by randomly varying the wind speed between 5 and 22 m/sec (which are the extreme values allowed by the UCL model).

- **Radiative transfer approximations.** The potential of the slanted-path plane-parallel approximation for the RT scheme has been deeply investigated (Roberti et al., 1994; Bauer et al., 1998; Kummerow, 1998). These authors generally agree on the errors being limited to a few K on average scenes, even though the local values may be important in case of large horizontal gradients (e.g., at the cloud edges) (see Liu et al., 1996; Czekala et al., 2000). We have compared the upwelling TBs at TMI frequencies and resolutions for the various cloud model simulations with the corresponding results generated by means of the 3-D Monte Carlo RT code of Roberti et al. (1994). Differences are usually limited to a few degrees except for the 85 GHz in correspondence of the most intense portions of the simulated storms, where the TBs computed with the slanted-path plane-parallel RT approximation may be up to about 20 K lower.

3.2.3 Microphysical constraints on cloud models from radiative analysis

We have explored the potential of the UW-NMS cloud model to reproduce the cloud structures of the simulated events by *statistically* comparing the computed TBs for the hurricane Bonnie simulation with the actual TMI measurements. It turns out that the simulated TBs show excessive cooling at 85 and 37GHz and excessive heating at 10 GHz, which may be due to the combination of several effects, such as a too large production of rain/ice precipitating hydrometeors by the cloud model -- especially in the most intense portions of the simulation --, or to its simplified description of the microphysical parameters of the various hydrometeor species. Based on comparisons carried out using different rain and graupel PSDs to compute the simulated TBs, the cloud model has been re-run (for a short period) with constant-slope Marshall-Palmer PSDs having slopes equal to 2.5 mm^{-1} for both hydrometeors and with an enhanced graupel density of 0.9 g/cm^3. As a result, an appreciable decrease (up to about 10%) of the largest values of both rain and graupel columnar contents has been observed in the new simulation, which produces a 30% improvement of the MI value when the simulated TBs are computed with the new PSDs and graupel density.

These results seem very promising, suggesting that a back-and-forth process of TB calibration/validation may provide extremely useful information for tuning the bulk microphysics of the mesoscale models.

4. Bayesian estimation methods

Almost all rainfall estimation techniques using microwave measurements present a probabilistic approach due to the statistical nature of precipitating cloud parameters. Both our TMI and TMI-PR combined retrieval algorithms (BAMPR-P and BAMPR-C) are based on a Bayesian approach. Here, we will first sketch the theoretical foundations of the Bayesian method in the case only one sensor is used, then we will describe the extension of the algorithm to combine TMI and PR data (see also Di Michele et al., 2001a; 2001b). A more detailed description of the BAMPR implementation, shown Figs. 1 and 2, will be also given.

4.1 Using single sensor (TMI)

Using a vectorial notation, we indicate with $\mathbf{g}$ the geophysical (hydrometeor content) vector related to a cloud profile and with $\mathbf{t}_m$ the multispectral vector of TMI measurements.

In the framework of the Bayes estimation theory, a possible optimal estimation is the one which gives the maximum of the *a posteriori* conditional probability density function (pdf), $p(\mathbf{g}|\mathbf{t}_m)$; this estimate, $\mathbf{g}_{MAP}$, is given by:

$$\mathbf{g}_{MAP} = \mathrm{Max}\{p(\mathbf{g}|\mathbf{t}_m)\} \tag{4}$$

This represents the Bayesian criterion of the Maximum *A posteriori* Probability (MAP). From a numerical point of view, the implementation of (4) imposes the search of a histogram maximum. This algorithmic aspect can be very sensitive to the sampling and density of cloud structure parameters (and corresponding TBs) within the cloud-radiation database (Di Michele et al., 2001a).

To overcome these MAP difficulties, in our retrieval scheme we resort to the Bayesian criterion of Minimum Mean Square (MMS), where the estimate $\mathbf{g}_{MMS}$ is defined as the expected value of $\mathbf{g}$, given a set of measurements $\mathbf{t}_m$; i.e.:

$$\mathbf{g}_{MMS} = \mathrm{Mean}\{p(\mathbf{g}|\mathbf{t}_m)\} \tag{5}$$

or, explicitly:

$$\mathbf{g}_{MMS} = \int_0^\infty \mathbf{g}\, p(\mathbf{g}|\mathbf{t}_m)\, d\mathbf{g} = \langle(\mathbf{g}|\mathbf{t}_m)\rangle \tag{6}$$

where the angle brackets indicate an ensemble averaging. Moreover, it is also worth noting that the MMS algorithm can easily furnish a measure of its intrinsic accuracy, since it can be proved that:

$$\boldsymbol{\sigma}^2_{gMMS} = \langle[(\mathbf{g}|\mathbf{t}_m) - \langle(\mathbf{g}|\mathbf{t}_m)\rangle]^2\rangle \tag{7}$$

where $\boldsymbol{\sigma}^2_{gMMS}$ is the profile estimate variance vector. The MMS algorithm is also referred to as Minimum Variance algorithm because it can be shown that it corresponds to minimize the conditional variance of $\mathbf{g}$ given $\mathbf{t}_m$.

Using the Bayes theorem, $p(\mathbf{g}|\mathbf{t}_m)$ can be transformed in the following way:

$$p(\mathbf{g}|\mathbf{t}_m) = p(\mathbf{t}_m|\mathbf{g})\, p(\mathbf{g})/p(\mathbf{t}_m) = p[\varepsilon_t(\mathbf{g})]\, p(\mathbf{g})/p(\mathbf{t}_m) \tag{8}$$

where $p(\mathbf{g})$ is the *a priori* pdf due to $\mathbf{g}$, and $\varepsilon_t(\mathbf{g}) = [\mathbf{t}(\mathbf{g}) - \mathbf{t}_m]$ is the TB error vector with $\mathbf{t}(\mathbf{g})$ the simulated TB vector related to $\mathbf{g}$ by means of the adopted radiative transfer model (Pierdicca et al., 1996). Since ε_t takes into account not only the radiometric absolute accuracy, but also other possible sources of error due to the forward modeling, we assume that it is a zero-mean random variable with Gaussian distribution. Thus, Eq. (8) becomes:

$$-ln\,[p(\mathbf{g}|\mathbf{t}_m)] = \varepsilon_t^T \mathbf{C}_{\varepsilon t}\, \varepsilon_t - ln\,[p(\mathbf{g})] + c_t \qquad (9)$$

where $\mathbf{C}_{\varepsilon_t} = \mathbf{C}_{\varepsilon_{t,\,rad}} + \mathbf{C}_{\varepsilon_{t,\,mod}}$ is the covariance matrix of radiometric (rad) and model (mod) TB errors, "T" stands for matrix transposition, and c_t is a constant with respect to $\mathbf{g}$ (including the determinant of $\mathbf{C}_{\varepsilon t}$). A description of various sources of uncertainties is given in Sub-section 3.2.2, while a description of the impact of $\mathbf{C}_{\varepsilon_t}$ on the retrieval can be found in Di Michele et al. (2001a).

The inversion scheme for BAMPR-P is shown on the left side of Fig. 1. The first step is a screening phase, where land and coast pixels are removed, while the rainy ones are selected among the ones relative to the ocean. The rain/no rain discrimination is based upon the measured TBs using the same method of the TRMM official products. The second step consists in the identification of the rainfall regime, which is achieved by determining if the measured TBs belong to either the moderate or to the intense rainfall class of the cloud-radiation database. In the third step, the Bayesian MMS inversion algorithm is applied using only the selected class of the cloud-radiation database. Output products are the hydrometeor and/or precipitation-rate profiles, together with columnar LWCs and surface rain rates. The corresponding accuracy values can be computed according to Eq. (7).

4.2 Using combined sensors (TMI and PR)

To combine radar and radiometer measurements, the just-described Bayesian technique is extended by considering the measured reflectivities in the same way than the radiometric measurements (Marzano et al., 1999). The simulated multi-gate radar reflectivity factors (hereafter, simply reflectivities, Z's) are indicated by a vector $\mathbf{z}$ (in $mm^6\ m^{-3}$ or dBZ). Each element of $\mathbf{z}$ represents the attenuated average reflectivity Z_i relative to the i-th layer (i.e., to the range gate of the cloud model), as it would be observed by the space-borne radar. As explained in previous Sub-section 3.1, $\mathbf{z}$ is related to the cloud structure (i.e., to vector $\mathbf{g}$): thus, it will be referred to as a function $\mathbf{z}(\mathbf{g})$.

In order to make the comparison possible, the PR reflectivity measurements have been averaged within each couple of heights defining the various cloud model layers (results will be indicated by the vector $\mathbf{z}_m$). Under the assumption of coincidence between the radiometer and radar beams, we can build a vector of measurements which is the merging of radiometric and reflectivity data, so that the conditional *a posteriori* pdf $p(\mathbf{g}|\mathbf{t}_m,\mathbf{z}_m)$ can be expressed as follows in the combined case:

$$p\,(\mathbf{g}|\mathbf{t}_m, \mathbf{z}_m, \mathbf{a}_m) = [p(\mathbf{t}_m|\mathbf{g})\, p(\mathbf{z}_m|\mathbf{g})\, p(\mathbf{a}_m|\mathbf{g})\, p(\mathbf{g})] \,/\, p(\mathbf{t}_m, \mathbf{z}_m, \mathbf{a}_m) \qquad (10)$$

This approach is sometimes referred to as "tall-vector" method (TVM). Note that we consider the total path attenuation at 13.8 GHz as addition measurement since it can be estimated from surface reference technique (Meneghini et al., 2000).

4.2.1 Combined retrieval within TRMM: inside the common TMI-PR swath

The TVM is here introduced just as a reference, for its application to TRMM data is cumbersome due to the different scanning systems of TMI and PR: the TMI is conically scanning at 53° off-nadir, while PR is cross-track linearly scanning. A way to overcome this difficulty is to separate the combined inversion problem into two steps in cascade (see Fig. 2). In the first step, a TMI-derived estimation is performed by applying the BAMPR-P algorithm. In the second step, the PR-based retrieval is carried out assuming the TMI-derived hydrometeor profile as additional constraint. We will refer to this TMI-PR cascade (TPC) technique as BAMPR-C.

As already mentioned, the TMI estimated profiles are slanted -- rather than vertical, as it would be requested for a TVM coupling with the corresponding PR reflectivity profiles. Since we use a two-step approach, we can tackle this problem by associating to each PR reflectivity beam several TMI-estimated slanted profiles, by

taking for each altitude range the corresponding portion of the TMI profile that intersects the PR beam. This process, however, is carried out only above the freezing level (assumed to be at 4.5 Km in this paper) because the PR estimates basically benefit only of the TMI information on the ice portion of the precipitating cloud.

According to this idea, the conditional *a posteriori* pdf in the second step can be written as follows:

$$p(\mathbf{g}_C|\mathbf{g}_{TMI}, \mathbf{z}_m, \mathbf{a}_m) = [p(\mathbf{g}_{TMI}|\mathbf{g}_C)\, p(\mathbf{z}_m|\mathbf{g}_C)\, p(\mathbf{a}_m|\mathbf{g}_C)\, p(\mathbf{g}_C)] / p(\mathbf{g}_{TMI}, \mathbf{z}, \mathbf{a}_m) \quad (11)$$

where $\mathbf{g}_C$ and $\mathbf{g}_{TMI}$ are the combined PR-TMI estimate and the TMI estimate, respectively (note that the latter was indicated as $\mathbf{g}_{MMS}$ in Sub-section 4.1). By comparing Eqs. (10) and (11), it emerges that $\mathbf{g}_{TMI}$ (which is obtained from $\mathbf{t}_m$) replaces $\mathbf{t}_m$ itself as the radiometer-derived information to the measurement set.

4.2.2 Combined retrieval within TRMM: radar-swath synthetic broadening

TMI has a much larger swath than PR (760 km vs. 220 km). This raises a new intriguing issue in the synergetic retrieval methodology -- i.e., it becomes important to see if it is possible to synthetically "broaden" the PR swath in order to achieve an estimation accuracy fairly uniform across the TMI swath. In our approach, this is achieved by the addition of the physical information derived from PR to the cloud-model database to be used outside the swath (where only TMI is available), capitalizing on the combined radar-radiometer observations within the common swath. Specifically, a PR-calibration of the emerging TBs associated to each profile of the cloud-radiation database is performed inside the common swath by means of a new combined cascade – which we call PR-TMI cascade (PTC) phase of the technique --, in which the two steps described in the previous Sub-section 4.2.1 are reversed. Then, the PR-calibration is extended to all profiles of the database. Finally, the BAMPR-P algorithm is applied to the TMI observations outside the common swath using the PR-calibrated database.

In the PTC phase, the PR-based estimation is used as a constraint for the TMI-based retrieval. This choice has the advantage to give a product which is compatible with the one obtained by using the BAMPR-P algorithm. Thus, we can directly compare the TBs associated to the hydrometeor profiles $\mathbf{g}_{PTC}$ estimated by the PTC phase (which we call $\mathbf{t}(\mathbf{g}_{PTC})$) and $\mathbf{t}(\mathbf{g}_{TMI})$, i.e. the TBs corresponding to the hydrometeor profiles $\mathbf{g}_{TMI}$ estimated by BAMPR-P. Their difference $\Delta\mathbf{t}$

$$\Delta\mathbf{t} = \mathbf{t}(\mathbf{g}_{PTC}) - \mathbf{t}(\mathbf{g}_{TMI}) \quad (12)$$

is due to the additional information derived from PR measurements in the common swath. The differences $\Delta\mathbf{t}$ can be used to build a regression-based relationship linking them to corresponding TMI measurements; i.e.:

$$\Delta\mathbf{t} = \mathbf{D}\,\mathbf{t}_m \quad (13)$$

where $\mathbf{D}$ is the regression coefficient matrix. This means that we can "calibrate" the simulated TBs as follows:

$$\mathbf{t}_{cal}(\mathbf{g}) = \mathbf{t}(\mathbf{g}) + \mathbf{D}\,\mathbf{t}(\mathbf{g}) \quad (14)$$

As a consequence, outside the common swath we replace the simulated $\mathbf{t}(\mathbf{g})$ with $\mathbf{t}_{cal}(\mathbf{g})$ given by Eq. (14). Noteworthy, this technique resembles that one described by Marzano et al. (1999) for a TVM approach. Obviously, this PR-calibration is reasonable only when the TB-pattern is homogeneous across the TMI swath. Thus, a pattern recognition method should be used in conjunction with this technique.

According to the Bayes theorem and similarly to Eqs. (8) and (11), the swath-broadening retrieved profile $\mathbf{g}_{SB}$ has to satisfy the following *a posteriori* pdf expression:

$$p(\mathbf{g}_{SB}|\mathbf{t}_m) = [p(\mathbf{t}_m|\mathbf{g}_{SB})\, p(\mathbf{g}_{SB})] / p(\mathbf{t}_m) = [p(\varepsilon_{tcal})\, p(\mathbf{g}_{SB})] / p(\mathbf{t}_m) \quad (15)$$

where the "calibrated" model error ε_{tcal} is:

According to the Bayes theorem and similarly to Eqs. (8) and (11), the swath-broadening retrieved profile $\mathbf{g}_{SB}$ has to satisfy the following *a posteriori* pdf expression:

$$p(\mathbf{g}_{SB}|\mathbf{t}_m) = [p(\mathbf{t}_m|\mathbf{g}_{SB})\, p(\mathbf{g}_{SB})] / p(\mathbf{t}_m) = [p(\boldsymbol{\varepsilon}_{tcal})\, p(\mathbf{g}_{SB})] / p(\mathbf{t}_m) \tag{15}$$

where the "calibrated" model error $\boldsymbol{\varepsilon}_{tcal}$ is:

$$\boldsymbol{\varepsilon}_{tcal} = \mathbf{t}_m - \mathbf{t}_{cal}(\mathbf{g}) \tag{16}$$

Eq. (15) represents the extension of Eq. (8) in the case of the swath broadening performed by using a PR-calibration approach for the cloud-radiation database. This technique has been numerically tested on synthetic data, but not yet applied to TRMM measurements. Results will be shown in a forthcoming paper (Di Michele et al., 2001b).

5. Applications to TRMM data

Extensive production of data has been made in the context of the EuroTRMM project, for the following sets of selected cases:

- Hurricane Bonnie (Atlantic Ocean – August 24-26, 1998)
- Hurricane Astrid (Atlantic Ocean – December 24-31, 1999)
- Wide-spread convective cases over the Atoll region (Pacific Ocean – August 8-September 4, 1998).

In what follows, we will focus on the TMI granule 4267 of August 25, 1998, when TRMM passed over hurricane Bonnie in the most intense period of the cyclone evolution. This case provided the best results when compared to the PR measurements, while the largest differences have been observed for the Atoll cases.

Fig. 8 shows the TMI images of hurricane Bonnie (granule 4267) at 10, 19, 37 and 85GHz, vertical polarization. The nadir cross-section of the measured TBs is shown in Fig. 9 together with the measured PR reflectivities. It is apparent that the observed scene is fairly composite, with a strong updraft embedded within a large stratiform region around 600 km in the along-track direction.

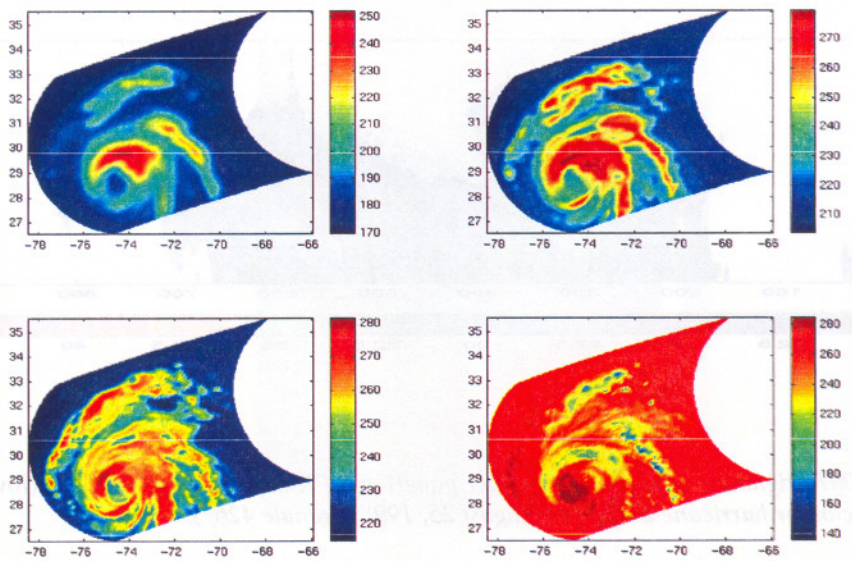

Fig 8: Hurricane Bonnie as seen from TMI on August 25, 1998 (granule 4267) at 10 GHz (upper left panel), 19 GHz (upper right), 37 GHz (lower left) and 85 GHz (lower right). Vertical polarization.

This case is really peculiar because of the very pronounced tilting of the convective tower, evidenced by the 10 km shift between the corresponding PR reflectivity peak and the TB deep minimum at 85GHz (see Hong et al., 2000 for more details on this event). Noteworthy, also the various TMI measurements at the different frequencies are shifted with respect to each other.

5.1 Using single sensor (TMI)

The upper panel of Fig. 10 shows the surface rain rates estimated with our algorithm BAMPR-P for the nadir section of hurricane Bonnie that has been shown in Fig. 9. Results are shown together with the estimation uncertainties, and compared with the official TRMM estimates for TMI (2A12 product). A systematic overestimation of the 2A12 with respect to BAMPR-P is evident. In addition, there is a slight displacement of the rainfall peak around 600 Km, which seems to be associated to the shift between the measured TBs, that has been pointed out in Fig. 9. While the 2A12 estimates appear to be more related to the 85 GHz measurements, the BAMPR-P estimates are more related to the lower frequencies. In the lower panel of Fig. 10, our estimates are shown together with the corresponding PR product (2A25). The shift of the rain rate peak is well evident as a consequence of the tilting described above. While the rainfall rate produced by the convective tower is severely underestimated by BAMPR-P and the rainfall appear to be distributed over a larger area -- a discrepancy that reflects the different resolution of the two estimates: 4 by 4 Km for 2A25, and 13 by 15 Km for BAMPR-P --, a very good agreement can be appreciated in the stratiform regions in spite of the different geometry and resolutions of the PR and TMI observations.

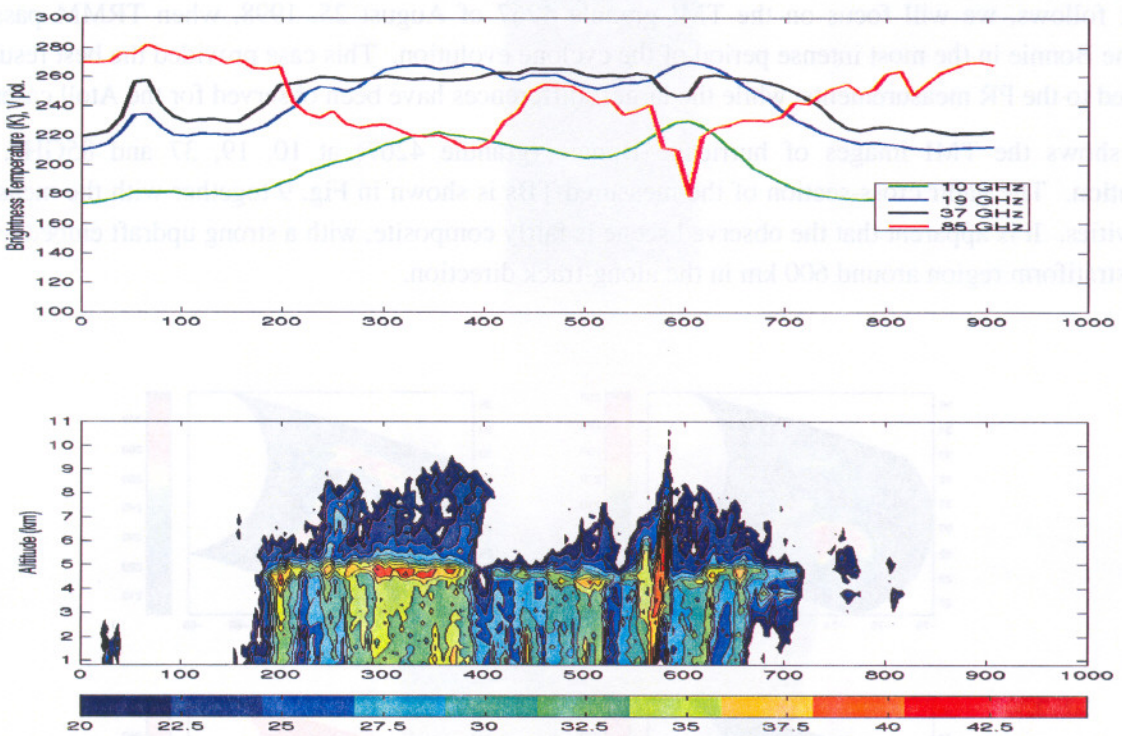

Figure 9: TMI brightness temperatures (upper panel) and PR measured reflectivities (lower panel) along the central scan for hurricane Bonnie on August 25, 1998 (granule 4267).

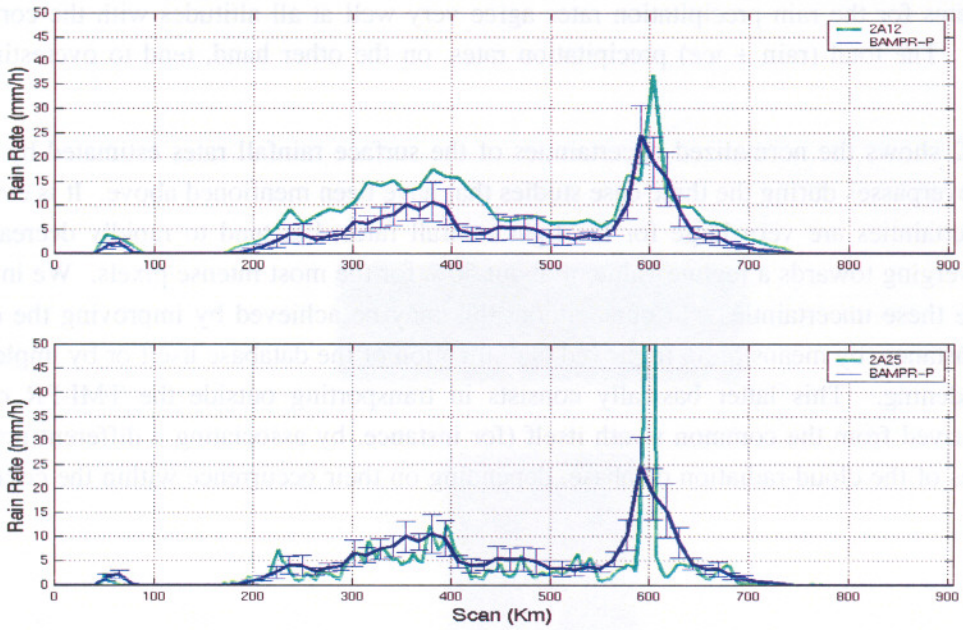

Fig 10: BAMPR-P surface rainfall rate estimates (mean and variance), together with 2A12 estimates (upper panel) and with 2A25 estimates (the lower panel), along the central scan of hurricane Bonnie on

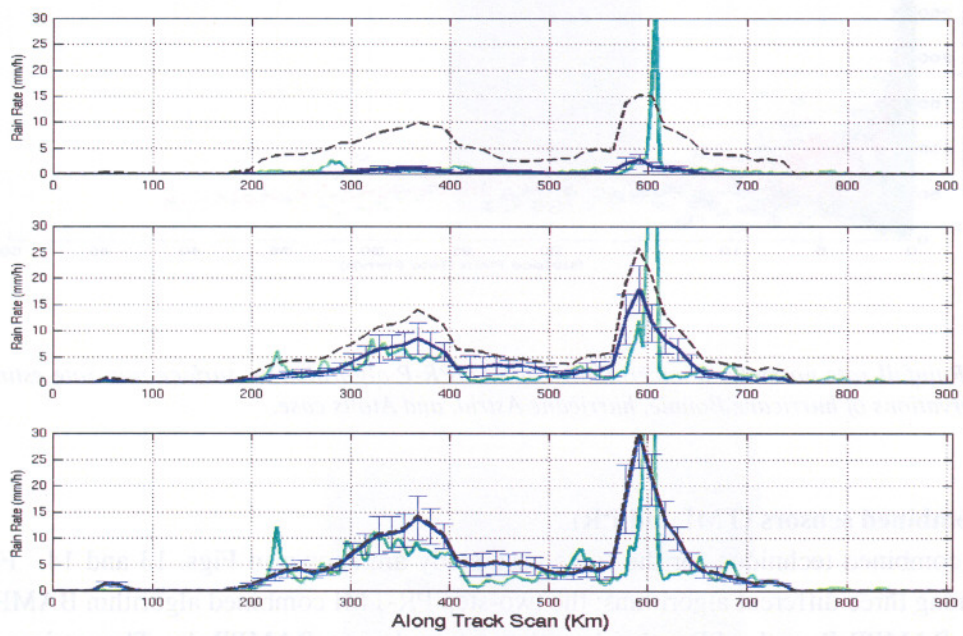

August 25, 1998.

Fig 11: BAMPR-P rain precipitation-rate estimates (blue line: mean and variance) for the layers (from bottom to top) 2.5 - 4 km, 4 - 5.5 km, and 5.5 - 7 km. In each panel, the cian line corresponds to the 2A25 estimate, while the dashed line refers to the BAMPR-P total (rain + ice) precipitation-rate estimate.

Differently to most passive-microwave rainfall algorithms, BAMPR-P estimates the precipitation rate profiles in addition to the surface rainfall rate. Thus, comparison with 2A25 products has been performed at higher altitudes as well. To this end, the precipitation rate profiles estimated with both 2A25 and BAMPR-P have been vertically averaged into five layers (0 – 2.5 km; 2.5 - 4.0 km; 4.0 - 5.5 km; 5.5 - 7 km; and above 7 km).

The three panels of Fig. 11 show the results for the three mid-layers. The most striking feature of this figure is that our estimates for the rain precipitation rates agree very well at all altitudes with the corresponding PR measurements. The total (rain + ice) precipitation rates, on the other hand, tend to overestimate the 2A25 products.

Finally, Fig. 12 shows the normalized uncertainties of the surface rainfall rates estimated by BAMPR-P for three TRMM overpasses during the three case studies that have been mentioned above. It is evident that in all cases, the uncertainties are very large for the light rainfall rates, but tend to rapidly decrease as rain rate increases, converging towards a regime value of about 50% for the most intense pixels. We intend to explore ways to reduce these uncertainties. In our opinion, this may be achieved by improving the cloud-radiation database: for instance, by means of an improved classification of the database itself or by implementing a sort of swath broadening. This latter basically consists in transporting outside the TMI-PR common swath information derived from the common swath itself (for instance, by associating a different probability to the cloud structures of the cloud-radiation database, depending on their occurrence within the combined TMI-PR retrievals).

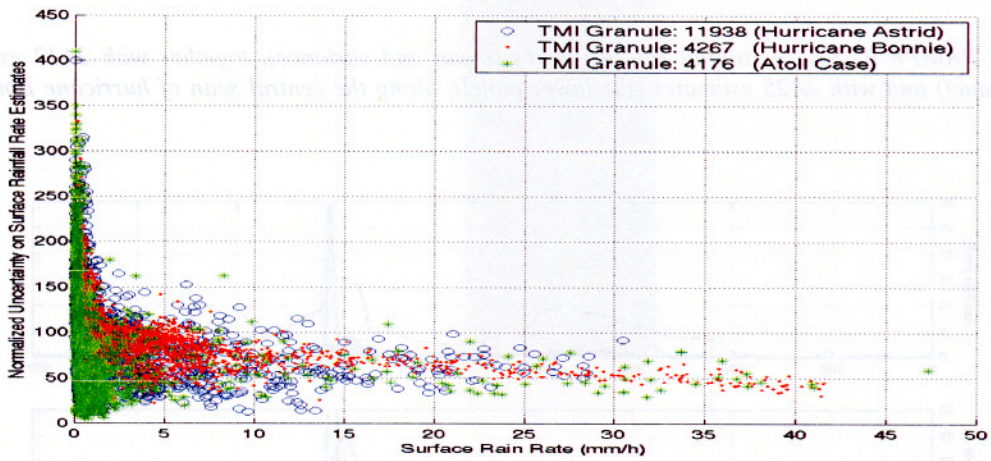

Fig 12: Rainfall-rate normalized uncertainties of BAMPR-P algorithm vs. surface rain rate estimates, for TMI observations of hurricane Bonnie, hurricane Astrid, and Atolls case.

5.2 Using combined sensors (TMI and PR)

Results of the combined technique for the same case study are shown in Figs. 13 and 14. Fig. 13 shows a comparison among three different algorithms: the two-step PR-TMI combined algorithm BAMPR-C, the TMI-only algorithm BAMPR-P, and a PR-only algorithm referred to as BAMPR-A. The retrieved ice columnar content is plotted in the upper panel, which evidences that the addition of ice content information from TMI drives the PR-only retrievals towards the TMI estimates. This, however, is less true for the surface rain rate retrievals shown in the lower panel since the combined retrieval is less sensitive to surface rain rate information provided by the TMI. In this case, the main effect of adding TMI information is to reduce the high peaks that are present in the PR-only retrievals.

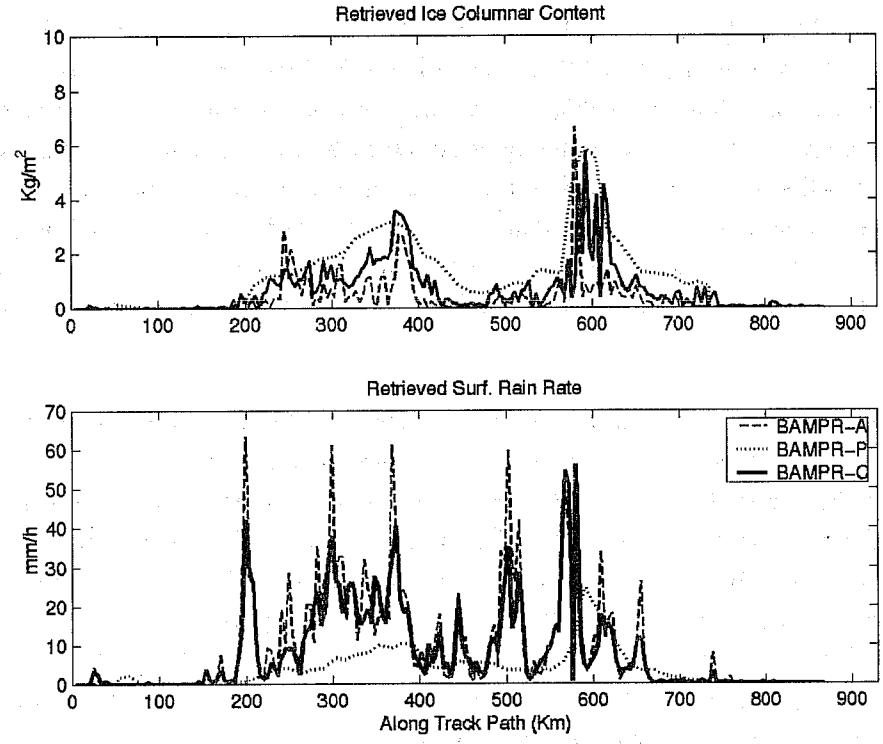

Fig 13: Comparison of the columnar ice (upper panel) and surface rain rate (lower panel) estimates performed using our TMI-only (dotted line), PR-only (dashed line), and combined TMI-PR algorithms along the central scan of hurricane Bonnie on August 25, 1998.

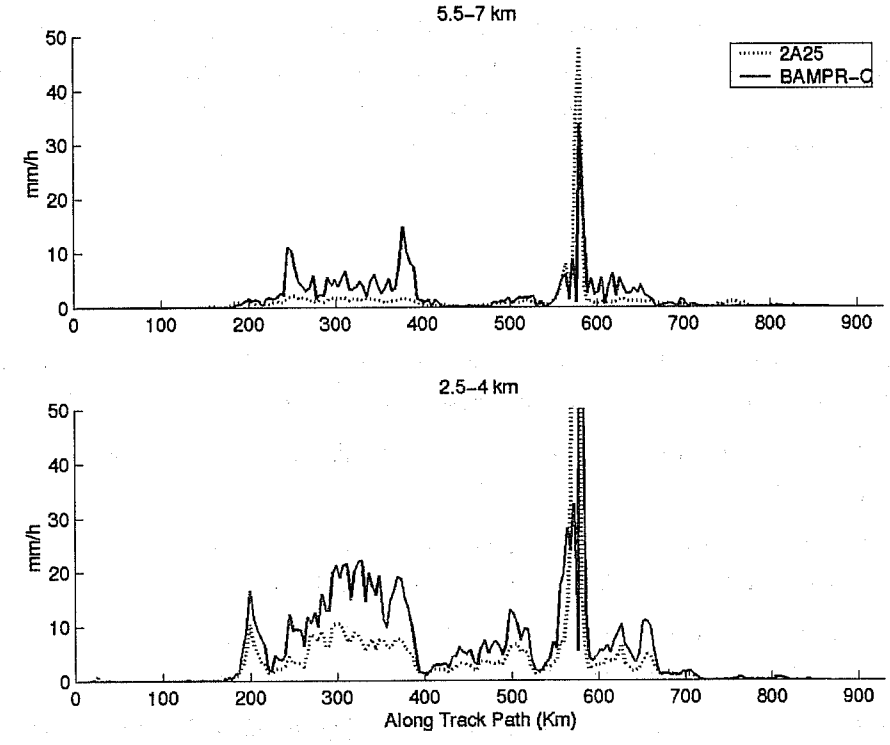

Fig 14: Comparison of BAMPR-C and 2A25 vertically-averaged rain and ice precipitation rates. Rain precipitation rates refer to the 2.5 – 5.0 km layer (lower panel) and ice precipitation rates to the 5.0 – 7.0 km layer (upper panel).

Fig. 14 shows an intercomparison between the two-step PR-TMI combined algorithm BAMPR-C and the official PR algorithm (2A25) (Iguchi et al., 2000). Vertically averaged results are shown for two layers (2.5 - 4.0 km; 5.5 - 7 km). It is evident that BAMPR-C overestimates 2A25 at almost every pixel. If we compare these results with the corresponding ones of Fig. 11, we see that while the combined algorithm BAMPR-C captures better both the convective peak and the ripple structure that are present in the 2A25 retrieval, the TMI-only retrieval BAMPR-P is (considerably) closer to the official product in the stratiform regions. In our opinion, the worse performance of the combined algorithm in the stratiform portions of the observed system is related to the fact that no bright band has been modeled within our cloud-radiation database. Thus, we plan to insert melting particles in the simulations to obtain reflectivity profiles that are closer to the observed ones.

6. Conclusions

The methodological features of a Bayesian inversion method (BAMPR), trained by 3-D cloud-resolving models combined with 3-D radiative transfer models, have been extensively investigated. Microphysical and radiative aspects of the forward problem have been discussed by stressing the implications of modeling assumptions upon the retrieval algorithm expected accuracy. The BAMPR algorithm has been applied and tested over several TRMM cases. In particular, the case of the hurricane Bonnie on August 25, 1998 has been analyzed in detail by comparing our results with the official TRMM products. Generally, precipitation rates estimated with BAMPR algorithm for TMI measurements only (BAMPR-P) tend to be in good agreement with PR official products, however, surface rainfall rates are usually lower than those estimated by the TMI official algorithm. The TMI-PR combined algorithm (BAMPR-C), on the other hand, does not perform well in the stratiform regions due to the lack of a melting layer within our RT simulations.

Acknowledgements. This work has been supported by European Union through EuroTRMM project (1997-2000). We want to thank Prof. Gregory Tripoli and Dr. Giulia Panegrossi of the University of Wisconsin for providing the hurricane Bonnie simulation and for profitable interactions. Thanks to Prof. Eric A.Smith of Florida State University for helpful discussions and to Dr. William Olson of NASA/Goddard Space Flight Center for providing portion of data of the TOGA-COARE simulation. Thanks to the EuroTRMM community and especially to Dr. Pedro Poiares Baptista. Thanks to our colleagues at IFA, Stefano Dietrich, Emma D'Acunzo and Cristophe Accadia for contributing the early stage of the work. A special appreciation to Laura Roberti for instructive collaboration.

References

Anagnostou, E.N., and C. Kummerow, 1997: Stratiform and convective classification of rainfall using SSM/I 85GHz brightness temperature observations. *J. Atmos. Oceanic Technol.*, **14**, 570-574.

Bauer, P., L. Schanz, and L. Roberti, 1998: Correction of the three-dimensional effects for passive microwave remote sensing of convective clouds. *J. Appl. Meteor.*, **37**, 1619-1632.

Bauer, P., A. Khain, I. Sednev, R. Meneghini, C. Kummerow, and F.S. Marzano, 2000: Combined cloud-microwave radiative transfer modeling of stratiform rainfall. *J. Atmos. Sci.*, **57**, 1082-1104.

Cotton, W.R., M.A. Stephens, T. Nehrkorn, and Tripoli G.J., 1982: The Colorado State University three-dimensional cloud/mesoscale model. Part II: An ice parameterization. *J. Rech. Atmos.*, **16**, 295-320.

Czekala, H., P. Bauer, D. Jones, F. Marzano, A. Tassa, L. Roberti, S. English, J.P.V. Poiares Baptista, A. Mugnai, and C. Simmer, 2000: Clouds and Precipitation. *COST Action 712: Radiative transfer models for microwave radiometry – Final Report of Project 1*, C. Maetzler Ed., EUR 19543 EN, Directorate-General for Research, European Commission, Brussels, Belgium, 37-72.

Di Michele, S., F.S. Marzano, A. Mugnai, A. Tassa, G. Panegrossi, G.J. Tripoli, E.S. Smith, L. Roberti, and J.P.V. Poiares Baptista, 2001a: Space-borne passive microwave retrieval of oceanic tropical precipitation. Part II: Inversion algorithms and application to TMI data. *To be submitted.*

Di Michele, S., F.S. Marzano, A. Mugnai, A. Tassa, and J.P.V. Poiares Baptista, 2001b: Space-borne passive and active combined retrieval of oceanic tropical precipitation: inversion algorithms and application to TRMM data. *To be submitted.*

Evans, K.F., J. Turk, T. Wong, and G.L. Sthephens, 1995: A Bayesian approach to microwave precipitation profile retrieval. *J. Appl. Meteor.*, **34**, 260-279.

Flatau, P.J., G.J.Tripoli, J. Verlinde, and W.R. Cotton, 1989: The CSU-RAMS cloud microphysics module: general theory and code documentation. *Depart. of Atmos. Sciance, Paper N0 451, Colo. State University, Fort Collins*, 87 pages.

Haddad, Z.S., E.A. Smith, C.D. Kummerow, T. Iguchi, M.R. Farrar, S.L. Durden, M. Alves, and W.S. Olson, 1997: The TRMM Day-1 radar/radiometer combined rain-profiling algorithm. *J. Meteor. Soc. of Japan*, **75**, 799-809.

Hong, Y., C. Kummerow, and W.S. Olson., 1999: Separation of convective and stratifrom precipitation using microwave brightness temperatures. *J. Appl. Meteor.*, **38**, 1195-1213.

Hong, Y., J. Hafermann, W.S. Olson, and C. Kummerow, 2000: Microwave brightness temperatures from tilted convective systems. *J. Appl. Meteor.*, **39**, 983-998.

Houze, R.A., P.V. Hobbs, P.H. Herzegh and D.B. Parsons, 1979: Size distribution of precipitation particles in frontal clouds. *J.Atmos Sci.*, **36**, 156-162.

Iguchi, T., and R. Meneghini, 1994: Intercomparison of single-frequency methods for retrieving a vertical rain profile from an airborne or spaceborne radar data. *J. Atmos. Oceanic Technol.*, **11**, 1507-1516.

Kummerow, C., W.S. Olson, and L. Giglio, 1996: A Simplified Scheme for Obtaining Precipitation and Vertical Hydrometeor Profiles from Passive Microwave Sensors. *IEEE Trans. Geosci. Remote Sens.*, **34**, 1213-1232.

Kummerow, C., W. Barnes, T. Kozu, J. Shiue, and J. Simpson, 1998: The Tropical Rainfall Measuring Mission (TRMM) sensor package. *J. Atmos. Oceanic Technol.*, **15**, 809-817.

Kummerow, C., 1998: Beamfilling errors in passive microwave rainfall retrievals. *J. Appl. Meteor.*, **37**, 356-370.

Lemaire, D., 1998: *Non-fully developed Sea State Characteristics from Real-Aperture Radar Remote Sensing*. PhD thesis, Université Catholique de Louvain, Belgium.

Liu, Q., C. Simmer, and E. Ruprecht, 1996: Three-dimensional radiative transfer effects of clouds in the microwave spectral range. *J.Geophys. Res.*, **101**, 4289-4298.

Marshall, J.S., and W. McK. Palmer, 1948: The distribution of raindrops with size. *J. Meteor.*, **5**, 165-166.

Marzano, F.S., A. Mugnai, E.A. Smith, X. Xiang, J. Turk, and J. Vivekanandan, 1994: Active and passive remote sensing of precipitating storms during CaPE. Part II: Intercomparison of precipitation retrievals over land from AMPR radiometer and CP-2 radar. *Meteor. Atmos. Phys.*, **54**, 29-51.

Marzano, F.S., J. Turk, S. Dietrich, A. Mugnai, G. Panegrossi, N. Pierdicca, and E.A. Smith, 1995: Microwave multisensor rainfall retrieval applied to TOGA-COARE observations. *Proc. of IGARSS'95, Florence (Italy)*, 1512-1514.

Marzano, F.S., A. Mugnai, G. Panegrossi, N. Pierdicca, E.A. Smith, and J. Turk, 1999: Bayesian estimation of precipitating cloud parameters from combined measurements of spaceborne microwave radiometer and radar. *IEEE Trans. Geosci. Remote Sens.*, **37**, 596-613.

Meneghini, R., J.R. Wang, H. Kumagai, and T. Iguchi, 1994: Description of radar/radiometer method and its application to airborne measurements over stratiform rain. *Proc. of IGARSS'94, Pasadena (CA)*, 1773-1775.

Meneghini, R., H. Kumagai, J.R. Wang, T. Iguchi, and T. Kozu, 1997: Microphysical retrievals over stratiform rain using measurements from an airborne dual-wavelength radar-radiometer. *IEEE Trans. Geosci. Remote Sens.*, **35**, 487-506.

Meneghini, R., T. Iguchi, T. Kozu, L. Liao, K. Okamoto, J.A. Jones, and J. Kwiatkowski, 2000: Use of surface reference technique for path attenuation estimates from the TRMM Precipitation Radar. *J. Appl. Meteor.*, **39**, 2050-2070.

Mohr, I.K., J.Famiglietti, and E.J.Zipser, 1999: The contribution to tropical rainfall with respect to convective system type, size and intensity from 85GHz ice-scattering signature. *J.Appl. Meteor.*, **38**, 596-606.

Mugnai, A., H.J. Cooper, E.A. Smith and G.J. Tripoli, 1990: Simulation of microwave brightness temperatures of an evolving hail storm at SSM/I frequencies. *Bull. Amer. Meteor. Soc.*, **71**, 2-13.

Mugnai, A., E.A. Smith, and G.J. Tripoli, 1993: Foundations for statistical-physical precipitation retrieval from passive microwave satellite measurements. Part II: Emission source and generalized weighting function properties of a time dependent cloud-radiation model. *J. Appl. Meteor.*, **32**, 17-39.

Olson, W.S., C. Kummerow, G.M. Heymsfield, and L. Giglio, 1996: A method for combined passive-active microwave retrievals of cloud and precipitation parameters. *J. Appl. Meteor.*, **35**, 1763-1789.

Olson, W.S., C. Kummerow, Y. Hong, and W.K. Tao, 1999: Atmospheric latent heating distributions in the tropics derived from satellite passive microwave radiometer measurements. *J. Appl. Meteor.*, **38**, 633-664.

Olson, W.S., P. Bauer, N.F. Viltard, D.E. Johnson, W.-K. Tao, R. Meneghini and L. Liao, 2001: A melting-layer model for passive/active microwave remote sensing applications. Part 1 Model formulation and comparison with observations. *J. Appl. Meteor.*, **40**, 1145-1163.

Panegrossi, G., S. Dietrich, F.S. Marzano, A. Mugnai, E.A. Smith, X. Xiang, G. J. Tripoli, P.K. Wang, and J.P.V. Poiares Baptista, 1998: Use of cloud model microphysics for passive microwave-based precipitation retrieval: significance of consistancy between model and measurement manifolds. *J. Atmos. Sci.*, **55**, 1644-1673.

Pierdicca, N., F.S. Marzano, G. D'Auria, P. Basili, P. Ciotti, and A. Mugnai, 1996: Precipitation retrieval from spaceborne microwave radiometers using maximum a posteriori probability estimation. *IEEE Trans. Geosci. Remote Sens.*, **34**, 831-845.

Roberti, L., J. Haferman, and C. Kummerow, 1994: Microwave radiative transfer through horizontally inhomogeneous precipitating clouds. *J. Geophys. Res.*, **99**, 16707-16718.

Roberti, L., and C. Kummerow, 1999: Monte Carlo calculations of polarized microwave radiation emerging from cloud structures. *J. Geophys. Res.*, **104**, 2093-2104.

Schols, J.L., and J.A. Weinman, 1994: Retrieval of hydrometeor distributions over the ocean from airborne single-frequency radar and multi-frequency radiometric measurements. *Atmospheric Research*, **34**, 329-346.

Sekelsky, S.M., W.L. Ecklund, J.M.Firda, K.S.Gage, and R.E.McIntosh,1999: Particle size estimation in ice-phase clouds using multifrequency radar reflectivity measurements at 95, 33, and 2.8GHz. *J. Appl. Meteor.*, **38**, 5-28.

Smith, E.A., A. Mugnai, H.J. Cooper, G.J. Tripoli and X. Xiang, 1992: Foundations for statistical-physical precipitation retrieval from passive microwave satellite measurements. Part I: Brightness-temperature properties of a time-dependent cloud-radiation model. *J. Appl. Meteor.*, **31**, 506-531.

Smith, E.A., C. Kummerow, and A. Mugnai, 1994a: The emergence of inversion-type profile algorithms for estimation of precipitation from satellite passive microwave measurements. *Remote Sens. Rev.*, **11**, 211-242.

Smith, E.A., X. Xiang, A. Mugnai and G.J. Tripoli, 1994b: Design of an inversion-based precipitation profile retrieval algorithm using an explicit cloud model for initial guess microphysics. *Meteorol. Atmos. Phys.*, **54**, 53-78.

Smith, E.A., F.J. Turk, M.R. Farrar, A. Mugnai, and X. Xiang, 1997: Estimating 13.8-GHz path-integrated attenuation from 10.7-GHz brightness temperatures for the TRMM combined PR-TMI precipitation algorithm. *J. Appl. Meteor.*, **36**, 365-388.

Smith, E.A., J. Lamm, R. Adler, J. Alihouse, K. Aonashi, E. Barrett, P. Bauer, W. Berg, A. Chang, R. Ferraro, J. Ferriday, S. Goodman, N. Grody, C. Kidd, C. Kummerow, G. Liu, F.S. Marzano, A. Mugnai, W. Olson, G. Petty, A. Shibata, R. Spencer, F. Wentz, T.T. Wilheit, and E. Zipser, 1998: Results of WetNet PIP-2 projects. *J. Atmos. Sci.*, **55**, 1483-1536.

Tao, W.K., and S.T. Soong, 1986: A study of the response of deep tropical clouds to mesoscale processes: Three dimensional numerical experiments. *J. Atmos. Sci.*, **43**, 2653-2676.

Tassa, A., S. Di Michele, E. D'Acunzo, C.Accadia, S. Dietrich, A. Mugnai, F. Marzano, G. Panegrossi, and L. Roberti, 1999: Analysis of TRMM observations of heavy precipitation events. *Microwave Radiometry and Remote Sensing of the Earth's Surface and Atmosphere*, 6th Specialist Meeting, VSP Int. Sci. Pub., 371-377.

Tassa, A., S. Di Michele, F.S. Marzano, A. Mugnai, G. Panegrossi, G.J. Tripoli, E.S. Smith, L. Roberti, and J.P.V. Poiares Baptista, 2001: Space-borne passive microwave retrieval of oceanic tropical precipitation. Part I: Assessment of cloud-radiation database accuracy. *To be submitted.*

Testud, J., P. Amayenc, and M. Marzoug, 1992: Rainfall-rate retrieval from a space-borne radar: comparison between single-frequency, dual-frequency and dual-beam techniques. *J. Atmos. Oceanic Technol.*, **9**, 599-623.

Testud, J., S. Oury, R.A. Black, P. Amayenc, and X. Dou, 2001: The concept of "normalized" distribution to describe raindrop spectra: a tool for cloud physics and cloud remote sensing. *J. Appl. Meteor.*, **40**, 1118-1140.

Tokai, A., and D. Short, 1996: Evidence form tropical raindrop spectra of the origin of rain from stratiform versus convective clouds. *J. Appl. Meteor.*, **35**, 355-371.

Tripoli, G.J., 1992: An explicit three-dimensional non-hydrostatic numerical simulation of a tropical cyclone. *Meteor. Atmos. Phys.*, **49**, 229-254.

Tripoli, G.J., and W. Cotton, 1980: A numerical investigation of several factors contributing to the observed variable intensity of deep convection over South Florida. *J. Appl .Meteor.*, **19**,1037-1063.

Ulbrich, C.W., 1983: Natural variations in the analytical form of the raindrop size distribution. *J. Clim. Appl. Meteor.*, **22**, 3452-3459.

Walden, C.J., G. Kuznetsov, and A. R. Holt, 1999: *Scattering properties of hydrometeors: modeling requirements.* Interim report on contract ENV4-CT97-0421, 7 pp.

Wilheit, T., R. Adler, S. Avery, E.C. Barrett, P. Bauer, W. Berg, A. Chang, J. Ferriday, N. Grody, S. Goodman, C. Kidd, D. Kniveton, C. Kummerow, A. Mugnai, W. Olson, G. Petty, A. Shibata, E.A. Smith, and R.W. Spencer, 1994: Algorithms for the retrieval of rainfall from passive microwave measurements. *Remote Sens. Rev.*, **11**, 163-194.

Willis, P.T., and P. Tattelmenn, 1989: Drop-size distributions associated with intense rainfall. *J. Appl. Meteor.*, **28**, 3- 15.

Wu, R., and J.A. Weinman, 1984: Microwave radiances form precipitating clouds containing aspherical ice, combined phase, and liquid hydrometeors. *J. Geophys. Res.*, **89**, 7170-7178.